Electronic Supplementary Material (ESI) for Physical Chemistry Chemical Physics.

*Supporting Information*

# *In Situ* XAFS of Acid-Resilient Iridate Pyrochlore Oxygen Evolution Electrocatalysts Under Operating Conditions

David L. Burnett, Enrico Petrucco, Andrea E. Russell, Reza J. Kashtiban, Jonathan D.B Sharman and Richard I. Walton

## S1: Materials synthesis

To prepare $(Ca,Na)_{2-x}Ir_2O_6\cdot H_2O$, $CaO_2$, $IrCl_3\cdot 5H_2O$ and $Na_2O_2$ in a 1:1:4 molar ratio based on 1.4 mmol of Ir which were added to 10 ml of 10 M NaOH solution. The reaction was carried out in a 20 ml Teflon-lined hydrothermal autoclave at 240 °C for a period of 96 hours. $Ca(OH)_2$ by-product was removed by washing with nitric acid. It was found that $(Ca,Na)_{2-x}Ir_2O_6\cdot H_2O$ with a variety of particle sizes could be synthesised, when the reaction temperature was varied between 170-240 °C, with lower temperatures producing materials with smaller particle sizes.

The reference materials $IrO_2$ and $IrCl_3$ were used as supplied by Johnson Matthey, while $BaNa_{0.5}Ir_{0.5}O_{3-\delta}$ was prepared as in our previous work.[1]

## S2: Materials characterisation

Powder XRD was measured using a Panalytical X'Pert Pro MPD equipped with a curved Ge Johansson monochromator, giving pure Cu $K_{\alpha 1}$ radiation, and a solid state PiXcel detector. A step size of 0.013° was typically used with the time per step 750 s, from the powdered sample on a spinning flat-plate. Rietveld refinement was carried out using the GSAS software.[2]

**Table S1: Figure S1: Rietveld fitted parameters to $(Ca,Na)_{2-x}Ir_2O_6{\cdot}H_2O$ $Fd\bar{3}m$, *a* = 10.23978(5) Å**

| Atom | Site | *x* | *y* | *z* | Occ | $U_{iso}$ / Å$^2$ |
|---|---|---|---|---|---|---|
| Ca | 16*d* | 0.5 | 0.5 | 0.5 | 0.704(3) | 0.0132(8) |
| Na | 16*d* | 0.5 | 0.5 | 0.5 | 0.239(5) | 0.0132(8) |
| Ir | 16*c* | 0 | 0 | 0 | 1.000(1) | 0.00313(14) |
| O | 48*f* | 0.3380(3) | 0.125 | 0.125 | 1.000(7) | 0.0024(13) |
| O' | 8*b* | 0.375 | 0.375 | 0.375 | 1.002(8) | 0.032(4) |

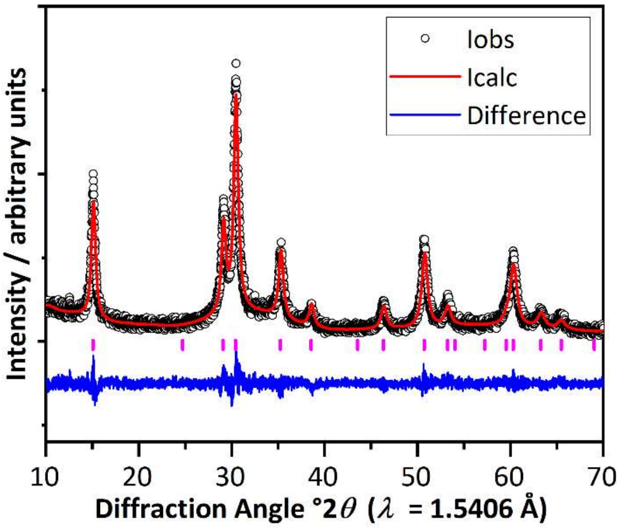

**Figure S1: Rietveld fit to powder XRD of small particle size $(Ca,Na)_{2-x}Ir_2O_6{\cdot}H_2O$ $Fd\bar{3}m$, *a* = 10.1981(11) Å**

Scanning transmission electron microscopy (STEM) analysis was carried out on a doubly corrected ARM200F microscope operating at 200 kV. Annular darkfield STEM (ADF-STEM) images were obtained using a JEOL annular field detector at a probe current of ~23 pA with a convergence semiangle of ∼25 mrad. EDXA measurements were carried out with an Oxford Instrument X-MaxN 100TLE windowless SDD to determine the elemental composition and distribution. BET surface areas.

Surface area measurements were carried out using a Micrometrics Tristar 3000 porosimeter with samples degassed under nitrogen at 200 °C for 12 hours and surface areas were calculated from the adsorption isotherms using BET theory.

Thermogravimetric analysis (TGA) combined with differential scanning calorimetry (DSC) was performed using a Mettler Toledo Systems TGA/DSC 1 instrument under a constant flow of air (50 mL min$^{-1}$). Data were recorded from room temperature to 1000 °C at a rate of 10 °C min$^{-1}$. Experiments were performed using a coupled mass spectrometry (MS): a Hiden HPR-

20 QIC R&D specialist gas analysis system, a triple filter mass spectrometer with SEM detection on heating in nitrogen was used to analyse water evolved from the materials. In this experiment the sample was held at 120 °C before continued heating to attempt to observe loss of surface water separately from crystal water. An initial mass loss of 4.8 % is observed, up to the end of the 4 hour hold at 120 °C, and can be attributed to the loss of surface water, as confirmed by the MS response and also shown by an exothermic feature in the DSC. At this point if it can be assumed that all the surface water has been removed, any further loss must be due to crystal water. Hence the next loss of 3.6 % of the remaining mass, can be attributed to the loss of crystal water, which is similar to the 3.2 % loss expected if the O’ site is fully occupied by $H_2O$, there is a small endothermic feature in the DSC overlapping this loss, meaning this is bound differently to the surface water lost at 120 °C, requiring an input of energy to remove water from within the crystal structure. There is a sharp endothermic peak in the DSC right after the loss of crystal water indicative of a second distinct mass loss, likely due to partial phase separation to a stoichiometric pyrochlore and $IrO_2$. The theoretical mass loss associated with reduction of iridium from +4.5 to +4 can account for approximately 3 % through loss of oxygen, not enough to match the observed loss. It is possible that during the phase change sodium is volatilised this would account for a further 2 % mass loss. Combining these two losses we come close to the loss observed experimentally. The loss observed at 750 °C can then be attributed to the formation of $CaIr_2O_4$ and reduction of the remaining iridium to metal.

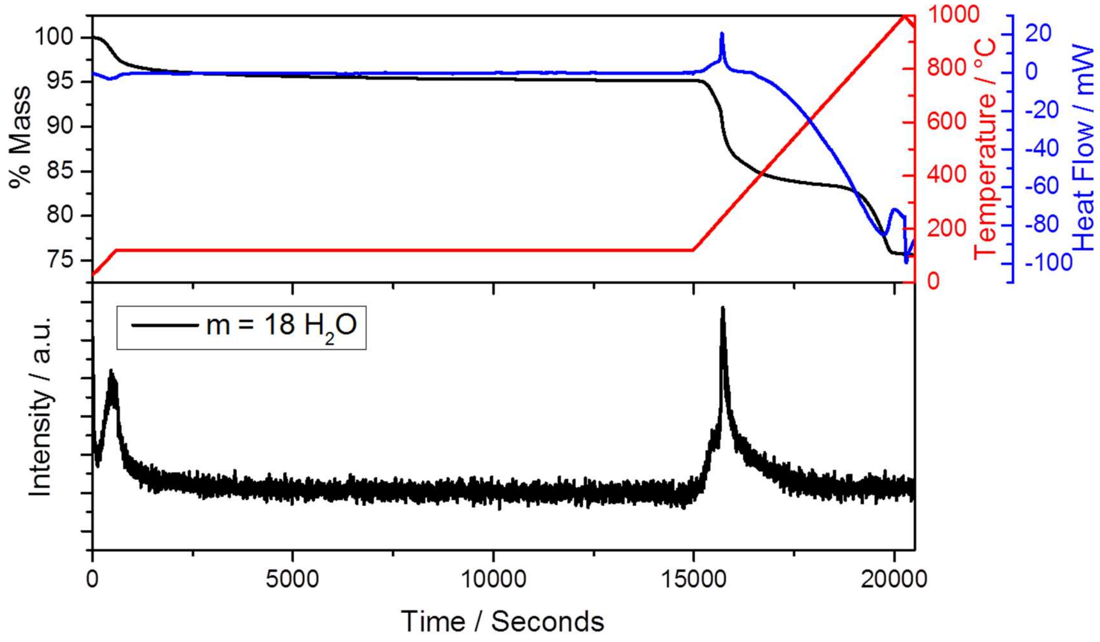

**Figure S2: TGA-MS of $(Ca,Na)_{2-x}Ir_2O_6 \cdot H_2O$**

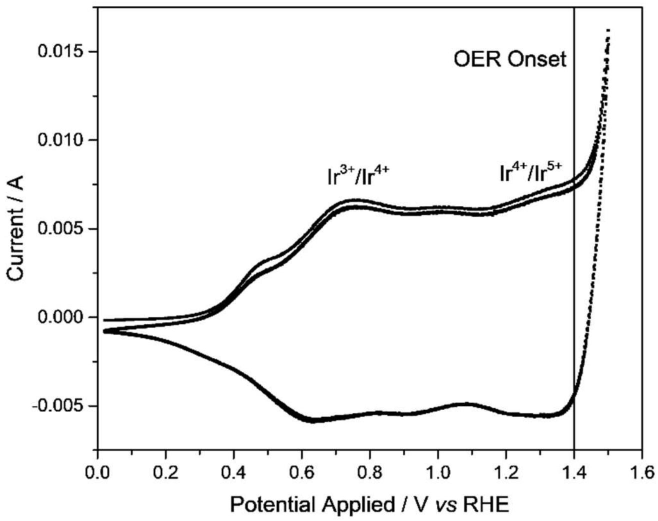

**Figure S3: Cyclic voltammogram of $(Ca,Na)_{2-x}Ir_2O_6{\cdot}H_2O$**

## S3: XAFS measurements

All experiments were performed on Beamline B18 of the Diamond Light Source, UK[3] at the iridium $L_{III}$-edge (≈11.2 keV) with XAFS spectra recorded from 11015.41 to 11813.81 eV. Incident energies were selected using a water-cooled, fixed-exit, double-crystal monochromator with Si(111) crystals. The spectra were recorded in QEXAFS mode. The beam was focussed horizontally and vertically using a double toroidal mirror, coated with Cr, 25 m from the source, while a pair of smaller plane mirrors were used for harmonic rejection. Static XANES spectra were recorded in transmission mode from samples diluted with polyethylene to give appropriate edge steps. *In situ* XAFS experiments were carried out in fluorescence mode using a 36-element germanium detector using a custom-made cell, Figure S3.[4]

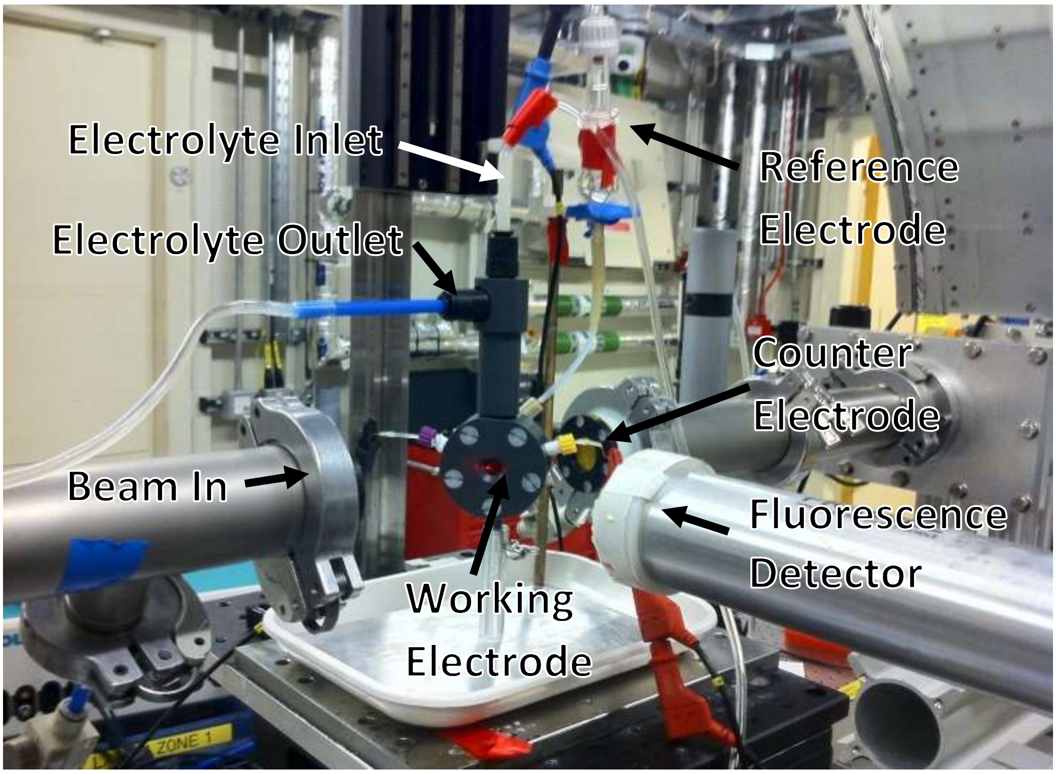

**Figure S4: Photograph of cell used to carry out *in situ* XAFS experiments.**

20 ml of 0.5 M $H_2SO_4$ was pumped around the cell using a non-pulsating pump, to avoid vibrations of the Kapton window, which would affect the quality of the collected data. A platinum counter electrode and a $Hg/Hg_2SO_4$ (MMS) reference electrode were used. Catalyst powders were mixed into inks using Nafion™ as a binder. These were then painted onto microporous layer coated carbon paper, Toray TGP-H-060, to fabricate electrodes. Electrodes were produced with loadings of approximately 0.5 mg cm$^{-2}$ of iridium. XANES + EXAFS spectra were recorded in fluorescence at chosen values of applied potential, with the electrode allowed to stabilise before data collection. Repeated scans were made at each potential and later any that showed excessive noise due to the interference of bubbles of evolving oxygen gas were discarded and the remaining normalised and summed to produce EXAFS spectra for analysis. The raw data were normalised using the software ATHENA[5] to produce XANES spectra and EXAFS spectra for modelling using the software ARTEMIS,[5] which uses the FEFF code for the calculation of phase shifts and effective scattering amplitudes, with starting structural models produced from published crystal structures to refine interatomic distances and thermal parameters. The XANES oxidation-state calibration was performed by taking the position of the white line (absorption energy maximum) as the edge position, as in our previous work on iridium oxides.[1] The $k^3$-weighted Ir $L_{III}$-edge EXAFS spectra were analysed over the k-range 3-12.5 Å$^{-1}$ using a single shell model. The contributions of shells of atoms at higher interatomic distances, even the Ir-Ca/Ir shell expected at ≈3.3 Å was found to be small and including these in the EXAFS fit did not change the conclusions from fitting the first shell alone. The coordination number of the shell was fixed at 6, and the interatomic distance and Debye-Waller factor were varied in least squares refinements. The threshold energy and

amplitude reduction factor, $S_0^2$, were also refined, and for the latter it always remained with 1 +/- 0.1, as expected and showed no systematic variation.

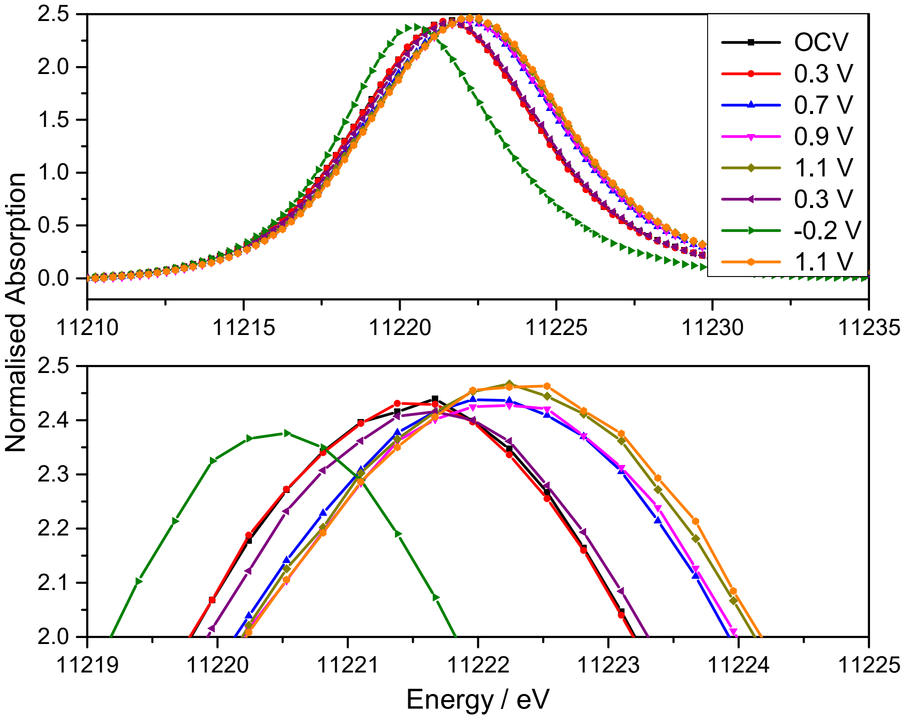

**Figure S5: Example of normalised *in situ* XANES showing white line shift of iridium $L_{III}$-edge and reproducibility upon reversal of potential (the legend denotes the order of the scans from top to bottom). Potentials are relative to the MMS reference electrode (0.68 V *vs* SHE).**

**Table S2: Fitted EXAFS parameters and XANES-derived oxidation state for *in situ* measurements on the large crystallite size $(Ca_{0.70}Na_{0.24})_2Ir_2O_6{\cdot}H_2O$.**

| **Applied Potential *vs* SHE / V (in sequence of experiment)** | **XANES oxidation state RW** | **EXAFS fitted parameters** | | | **EXAFS Bond Valence Sum*** |
|---|---|---|---|---|---|
| | | *d*(Ir-O) / Å | $\sigma^2$(Ir-O) | $S_0^2$ | |
| Open circuit | 4.42 | 1.977(20) | 0.0064(28) | 0.98 | 4.49 |
| 0.98 | 4.35 | 1.964(23) | 0.0052(31) | 0.89 | 4.66 |
| 1.18 | 4.51 | 1.945(22) | 0.0063(29) | 0.94 | 4.90 |
| 1.28 | 4.56 | 1.940(20) | 0.0054(26) | 0.98 | 4.97 |
| 1.38 | 4.64 | 1.927(32) | 0.0069(43) | 1.01 | 5.15 |
| 1.48 | 4.69 | 1.931(18) | 0.0044(24) | 0.86 | 5.08 |
| 1.58 | 4.71 | 1.928(24) | 0.0055(32) | 0.94 | 5.13 |
| 1.68 | 4.74 | 1.928(20) | 0.0045(26) | 0.87 | 5.12 |
| 1.78 | 4.73 | 1.931(18) | 0.0044(24) | 0.86 | 5.08 |
| 0.98 | 4.37 | 1.961(20) | 0.0062(28) | 0.94 | 4.69 |
| 0.48 | 3.56 | 2.042(15) | 0.0030(20) | 0.86 | 3.77 |

* Calculated using the bond valence parameter for Ir(IV) https://www.iucr.org/resources/data/datasets/bond-valence-parameters

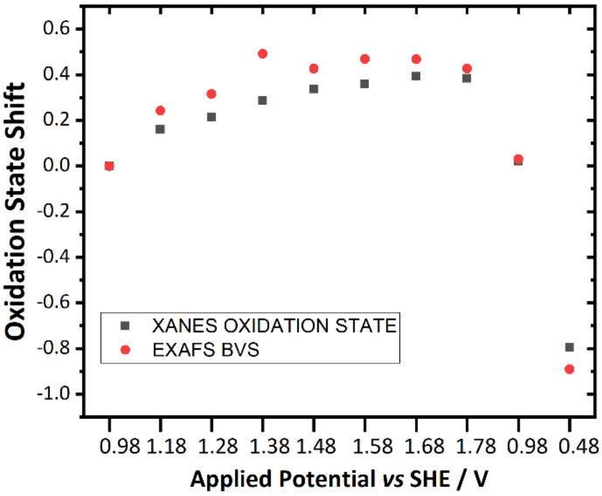

**Figure S6: Comparison of oxidation state shift from XANES and bond valence sum (BVS) analysis of EXAFS bond distances.**

## References

1 K. Sardar, E. Petrucco, C. I. Hiley, J. D. B. Sharman, P. P. Wells, A. E. Russell, R. J. Kashtiban, J. Sloan and R. I. Walton, *Angew. Chem., Int. Ed.*, 2014, **53**, 10960-10964.

2 A. C. Larson and R. B. V. Dreele, *General Structure Analysis System (GSAS), Los Alamos National Laboratory Report*, 1994, **LAUR 86-748**.

3 A. J. Dent, G. Cibin, S. Ramos, A. D. Smith, S. M. Scott, L. Varandas, M. R. Pearson, N. A. Krumpa, C. P. Jones and P. E. Robbins, *J. Phys. Conf. Ser.*, 2009, **190**, 012039

4 P.W. Richardson, “Oxygen evolution electrocatalysts for proton exchange membrane water electrolysis,” PhD Thesis, School of Chemistry, University of Southampton, 2015.

5 B. Ravel and M. Newville, *J. Synchrotron. Rad.*, 2005, **12**, 537-541.